

Searching from Area to Point: A Hierarchical Framework for Semantic-Geometric Combined Feature Matching

Yesheng Zhang, Xu Zhao
Department of Automation
Shanghai Jiao Tong University
Shanghai, China

Dahong Qian
School of Biomedical Engineering
Shanghai Jiao Tong University
Shanghai, China

Abstract—Feature matching is a crucial technique in computer vision. Essentially, it can be considered as a searching problem to establish correspondences between images. The key challenge in this task lies in the lack of a well-defined search space, leading to inaccurate point matching of current methods. In pursuit of a reasonable matching search space, this paper introduces a hierarchical feature matching framework: *Area to Point Matching* (A2PM), to first find semantic area matches between images, and then perform point matching on area matches, thus setting the search space as the area matches with salient features to achieve high matching precision. This proper search space of A2PM framework also alleviates the accuracy limitation in *state-of-the-art* Transformer-based matching methods. To realize this framework, we further propose *Semantic and Geometry Area Matching* (SGAM) method, which utilizes semantic prior and geometry consistency to establish accurate area matches between images. By integrating SGAM with off-the-shelf Transformer-based matchers, our feature matching methods, adopting the A2PM framework, achieve encouraging precision improvements in massive point matching (up to +24.98%) and pose estimation (up to +21.04%) experiments, outperforming all published methods.

I. INTRODUCTION

Feature matching is a fundamental task in computer vision, which supports a wide range of vision applications as simultaneous localization and mapping [1], structure from motion [2], image alignment [3], etc. Traditional methods [4], [5] employ the detector-based framework where keypoints are detected and described first, and then matched by nearest neighbor searching. As the technology evolves, learning-based approaches such as Convolution Neural Network (CNN) and Transformer [6] are used in feature matching either to replace some separate phases in the detector-based matching framework [7], or to establish point matches directly from the image pair [8], [9], i.e. adopting the direct matching framework.

In essence, feature matching can be treated as a searching problem to look for point matches between images, where the search space is the key factor affecting matching performance. A well-defined search space should be easily available and enable efficient searching by avoiding redundant and error-prone computation. The detector-based framework reduces the matching search space to keypoints between images for efficient matching. Detecting keypoints even with deep CNN [10], [11] in the image, however, suffers

from inaccurate and failed detection caused by rapid change in viewpoint, varied illumination, complex 3D geometry and motion blur. Thus recent direct matching framework performs dense matching between images to avoid detection failure, but remains the entire image as the search space. At the same time, in contrast to CNN with restricted receptive field [8], [12], [13], Transformer is more suitable for this framework and achieves SOTA performance [9], [14], [15], [16], as attention layers endow perception of global context. Nevertheless, keeping the search space as the entire image almost certainly leads to redundant computation in feature matching. To reduce the computational cost, the full-image attention computation has to be implemented in size-reduced images, in which much detailed information is lost, limiting the matching accuracy. Although effective search strategies are proposed [16], [15], [17], [18], full-image feature extraction and cross attention are still expensive due to the redundant search space. Therefore, existing frameworks lack in defining an appropriate search space which is crucial for precise feature matching.

To remedy this problem, the matching search space can be set to areas with prominent semantic contents in images, named semantic areas, such as the areas containing a complete object or an intersection of several different semantic entities. The reasons are as follows. **1)** The semantic areas between images can be easily matched, owing to the invariance of semantic to viewpoint, illumination and scale [19], [20], [21]. **2)** This area-level search space facilitates the feature matching, as stable image features supporting precise point matches are usually clustered in these semantic areas, like surfaces and edges of objects or the intersection of different entities. **3)** Area-based attention computation is more manageable than entire-image-based for Transformer-based methods, as the precision limitation is alleviated so that more accurate point matching can be achieved.

Based on the above analysis, a hierarchical feature matching framework: *Area to Point Matching* (A2PM, Fig.1 top) is proposed in this paper. It reduces the matching search space properly to semantic areas by finding semantic area matches between images first, and then performing point matching on matched areas. To achieve this search space reduction, we propose *Semantic Area Matching* (SAM), utilizing the semantic prior to efficiently detect and match

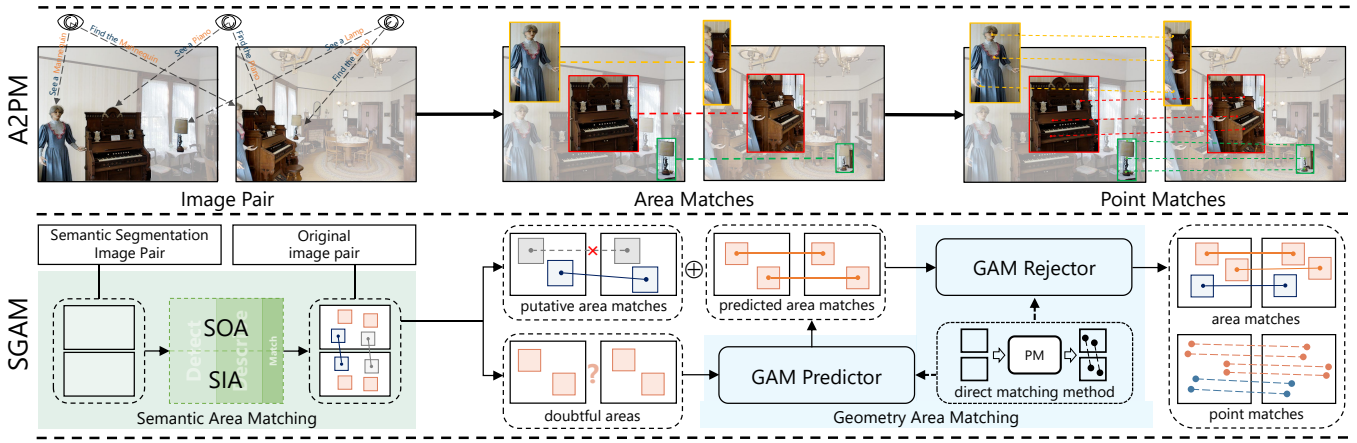


Fig. 1. **Overview of the proposed feature matching framework and area matching method.** (i) **Top:** The proposed *Area to Point Matching* (A2PM) framework first finds semantic area matches between images and then performs point matching on matched areas. (ii) **Bottom:** For area matching, we propose *Semantic and Geometry Area Matching* (SGAM) method including *Semantic Area Matching* (SAM, the green part) and *Geometry Area Matching* (GAM, the blue part). The SAM takes semantic segmentation to detect and match *semantic object area* (SOA) and *semantic intersection area* (SIA) between images. Integrating with a Point Matcher (PM), the GAM consists of a Predictor (GP) to determine true matches from doubtful areas and a Rejector (GR) to screen out false and bad area matches.

areas between images. But the semantic abstraction omitting local details may cause *semantic ambiguity* during matching, when different instances appear in the image together, which can not be handled by SAM. Thus we turn to the epipolar geometric constraint of point matches within the areas. Geometry consistency of area matches is therefore formed using fundamental matrices. It enables the proposed *Geometry Area Matching* (GAM) to integrate a direct matching method to construct the area geometry consistency. GAM allows to predict true area matches from doubtful candidates (GAM Predictor, GP), and to reject false and inferior area matches in SAM (GAM Rejector, GR).

By combining SAM and GAM, the *Semantic and Geometry Area Matching* (SGAM, Fig. 1 bottom) can achieve accurate area matching between images and realize the A2PM framework for precise feature matching. Specifically, SAM takes semantic segmentation images to detect and match two types of image areas: semantic object area and semantic intersection area. After a process of detection, description and matching, putative area matches and doubtful areas (which may occur in case of semantic ambiguity) are output by SAM. Then, GP predicts true area matches from doubtful areas according to geometry consistency. Finally, all area matches are fed into GR to obtain area matches with better geometry consistency and point matches within them.

In sum, the main technical contributions of this work are:

- 1) A hierarchical feature matching framework: A2PM, is proposed. It reduces the feature matching search space to area matches between images with prominent semantic distributions for high matching accuracy.
- 2) To reduce the search space, we propose SGAM approach for area matching, including SAM to find putative area matches utilizing semantic and GAM to refine precise area matches based on geometry consistency.
- 3) This novel framework shows excellent compatibility with Transformer-based direct matching methods by easing their accuracy limitations, attaining remarkable

matching precision improvement and *state-of-the-art* pose estimation performance in massive experiments.

II. RELATED WORK

Detector-based Matching. Feature matching is based on the detected image keypoints and their descriptors in this framework [4], [5]. By the descriptor distance minimization where nearest neighbor (NN) search is usually adopted, point matches are established between images. In the age of deep learning, recent work [22], [10], [23], [11], [24], [25], [26] turn to deep CNN to achieve better learning feature. Specifically, SuperPoint [24] is early to provide self-supervised feature detection and description networks and outperforms conventional methods. Subsequent D2Net [23] propose a unified network to detect and describe feature and ASLFeat [11] refines this network to obtain superior performance. Recent ALike [10] utilizes differentiable detection module to improve the localization accuracy for point matches. At the same time, detached learning detection [27], [28], [29] and description [30], [31], [32] are proposed as well. After feature detection, point matching including match searching and outlier rejection is also advanced by recent learning methods [33], [34], [35], such as SuperGlue [33] using graph neural network to learn more robust matches.

Direct Matching. In order to avoid detection failure, direct matching framework is proposed [8], [9], [14], which aims at jointly trainable feature detection, matching and outlier rejection to establish point matches directly from image pairs. At first, 4D CNNs are adopted to extract dense image feature [8], [12], [36]. Owing to limited receptive field [9] of CNN, recent direct matching methods [9], [14] adopt Transformer [6] to process dense feature extracted by CNN, attaining *state-of-the-art* performance. However, the global search space leads to redundant computation, restricting them from high resolution input image. Although recent work [37], [15], [16], [18], [17] has proposed more effective search strategy to improve the accuracy and speed, the precision limitation

due to redundant search space, i.e. the loss of detailed image information during input size reduction, remains unresolved. Thus, we effectively use available semantic information to perform area matching in images before point matching, alleviating computational redundancy and improving input resolution.

Area-based Solutions in Feature Matching. Hierarchical processing based on areas exists in many vision tasks. In feature matching, GMS [38] early notices the aggregation of solid point matches and utilizes support areas to reject outliers, but its area is tiny assuming small camera motion. When the camera viewpoint changes a lot, the large scale difference between images is the main problem in feature matching. Therefore, scale estimation methods [39], [40] with known or roughly determined co-visible areas are recently proposed to improve the matching performance. Recently, the overlap estimation method [41] is proposed to guide the feature matching, but its full Transformer-based network are computationally consuming. Our SGAM method focuses on finding area matches with specific semantic distributions, which naturally resolves the scale difference and effectively utilizes the easily accessible semantic information avoiding large computation costs.

III. FORMULATION

Given an image pair (I_0, I_1) and a query point $p \in I_0$, the process of A2PM framework (\mathcal{M}_A) is formulated as:

$$q_A = \mathcal{M}_A(p|I_0, I_1, PM) \stackrel{AM}{=} PM(p|\alpha, \beta) \quad (1)$$

where AM is the area matching method to achieve area matches $\alpha \in I_0$ and $\beta \in I_1$ with $p \in \alpha$, q_A is the matched point and PM is the Transformer embedded direct point matcher. Assuming α, β are matched accurately and contain salient features to support accurate point matching, compared to the direct matching framework (\mathcal{M}_D) with the same PM :

$$q_D = \mathcal{M}_D(p|I_0, I_1, PM) \stackrel{resize}{=} PM(p|I'_0, I'_1) \quad (2)$$

(I'_0, I'_1 are the resized images), \mathcal{M}_A can obtain more accurate point matching, as the search space is reduced properly and the accuracy limitation of PM is alleviated:

$$|q - q_D| > |q - q_A| \quad (3)$$

where q is the ground truth match point. Detailed derivations of Eq. 3 can be found in the supplementary material.

Area Matching with Geometry Consistency: To achieve this search space reduction, we further formulate the area matching and its geometry consistency. Suppose N area matches with prominent semantics exist between images:

$$\{A_{i\pi(i)}\}_i^N := \{(\alpha_i, \beta_{\pi(i)})\}_i^N \quad (4)$$

where $\pi(i) \in [0, R)$ is an one-to-one permutation and areas $\alpha_i \in I_0, \beta_{\pi(i)} \in I_1$. Then area matching is formulated as:

$$\{A_{i\pi(i)}\}_i^N = AM(I_0, I_1) \quad (5)$$

In order to construct its geometry consistency, we turn to the fundamental matrix constraint of point matches within areas.

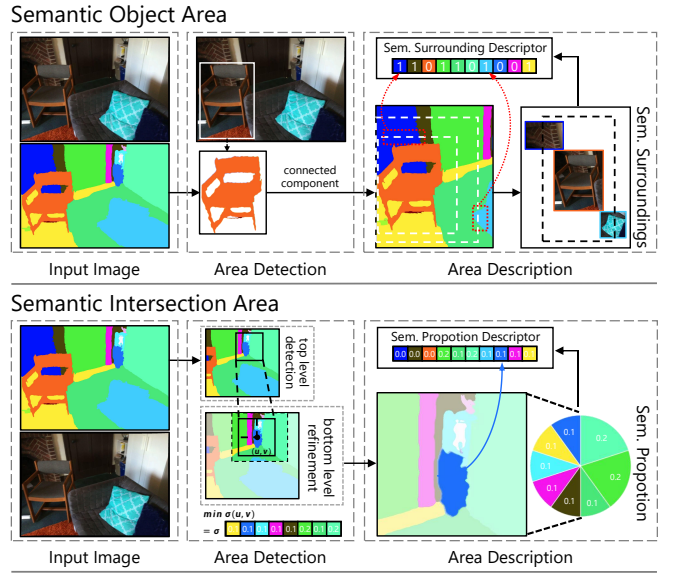


Fig. 2. **Semantic Area Matching (SAM).** SAM divides image areas into two types to process. For both types of areas, area detection and description are performed first, and then area matching is based on specially-designed descriptor distance minimization.

First, the correspondences $\mathcal{P}_i = \{(q_i^m, p_i^m)\}_m^M$ of $A_{i,\pi(i)}$ can be achieved by PM and the fundamental matrix F_i can be calculated as well. Then we form the geometry consistency between \mathcal{P}_i and F_i by Sampson distance [42]:

$$d_{i,i} = \sum_m \frac{(p_i^m F_i q_i^m)^2}{(F_i q_i^m)_1^2 + (F_i q_i^m)_2^2 + (F_i p_i^m)_1^2 + (F_i p_i^m)_2^2} \quad (6)$$

$$:= D(F_i, \mathcal{P}_i) \rightarrow 0$$

where $(A)_k$ represents the k -th entry of the vector A . It should be ideally closed to 0 and reflects the matching precision of $A_{i,\pi(i)}$, since only the correct area match will produce accurate point matches. Similarly, we can deduce the geometry consistency across area matches. Given two correct area matches $\{A_{i,\pi(i)}, A_{j,\pi(j)}\}$, they should generate correspondences with similar fundamental matrices. Thus the cross Sampson distance ($d_{i,j}$) should be close to 0:

$$d_{i,j} = D(F_i, \mathcal{P}_j) \rightarrow 0 \quad (7)$$

Therefore, in an area match set $\{A_{i,\pi(i)}\}_i^N$, assuming most of area matches are correct, the geometry consistency of a specific area match $A_{i,\pi(i)}$ can be formulated as:

$$G_{A_{i,\pi(i)}} = \frac{1}{N} \sum_j d_{i,j} \quad (8)$$

Thus, the $G_{A_{i,\pi(i)}}$ can reflect the matching accuracy of $A_{i,\pi(i)}$ and the smaller the higher area matching precision.

IV. SEMANTIC AREA MATCHING

Semantic is an essential cue for area detection and matching, because areas containing solid image feature usually possess specific semantic distributions, namely, semantic areas. Therefore, we define two kinds of semantic areas as:

1) Semantic Object Area: the area containing single object with a textured surface or distinguished edges generating stable image feature; **2) Semantic Intersection Area:** the area where different semantic entities meet, including solid image feature due to the appearance change in the intersection. Then, the proposed *Semantic Area Matching* (SAM, Fig.2) is to detect and match the above two types of areas from semantic segmentation image (I^s), adopting a process of detection, description and matching.

A. Semantic Object Area

The semantic object area is centered on the object which always contains solid image feature. It is extracted from I^s by the object connected components and described through the semantic surroundings in SAM (Fig. 2 top).

Area Detection. Detecting semantic object areas is easy by finding the connected components with the object semantic in I^s and setting their bounding boxes as the area boundaries. To achieve sparse extraction, we fuse the spatially close areas with the same semantic.

Area Description. Since the semantic object area already has the object semantic, its descriptor is to distinguish different instances. As the close instances are merged in the area detection, only spatially scattered instances need to be distinguished, which probably have different surroundings. So we propose the *semantic surrounding descriptor*, which utilizes the surrounding semantics to achieve instance differentiation. This descriptor is firstly constructed as a binary zero vector, where each bit represents a semantic in the image pair. Then, we record all the semantics passed by the area boundaries and set the corresponding bits in the binary vector to one to obtain the final descriptor. After that the area matching can be performed by minimization the hamming distance of these descriptors.

Specificity Enhancement. To better collect the surroundings, the descriptors can be formed on multiscale boundaries and merged together by a binary *OR* operation. To improve the specificity, it is optional to construct a descriptor on each side of the area boundary. Then the final descriptor is integrated by four side descriptors in a fixed order, but it is more sensitive to the camera view.

B. Semantic Intersection Area

The semantic intersection area contains intersections of various semantics, possessing salient features due to appearance change. It is extracted on the semantic pyramid and described using semantic proportions (Fig. 2 bottom).

Area Detection. The core of detecting semantic intersection areas is sliding the area window on I^s to collect locations where the area contains enough amount of semantics, e.g. more than 3 semantics. Non-maximum suppression is used for sparse detection. As direct sliding window results in huge time consumption, we use a two-layer semantic pyramid. The top layer is the I^s reduced to scale r . The

area window slides over it for initial detection. The bottom layer is the original I^s , used to refine the area location. In refinement, we first calculate the proportions of semantics in each area. To keep prominent features close to the area center, the variance σ of all semantic proportions in the area is minimised to adjust the area location.

Area Description. Since semantics within the area is key to identify the same semantic intersection area across images, we propose the *semantic proportion descriptor*, which describes the semantic proportion in the area. This descriptor is a vector where each bit represents a semantic in the image pair and the value of each bit is the proportional value of the corresponding semantic in the area.

Scale and Specificity. To improve the scale invariance, the descriptors can be constructed on multiscale areas and merged together by taking the average. The spatial specificity can also be enhanced by quartering original area from the center and forming descriptors for each subarea to compose the final descriptor in a fixed order.

V. GEOMETRY AREA MATCHING

Although SAM works well in most cases, ignoring local details in images may lead to *semantic ambiguity* when different instances simultaneously occur in the image pair. Especially when their semantic surroundings are similar, SAM may obtain doubtful areas and incorrect area matches. On the other hand, like point matches, area matches are also constrained by the epipolar geometry which can be used to handle the semantic ambiguity. Thus, based on the geometry consistency formulated in Sec. III, we propose *Geometry Area Matching* (GAM) to refine the results of SAM and fulfil the A2PM framework, including a predictor to determine true matches from doubtful areas and a rejector to screen out false and inferior area matches.

A. Geometry Area Match Predictor

The GAM Predictor (GP) aims to determine the true matches among multiple matching possibilities caused by semantic ambiguity. Given areas $\{\alpha_i\}_i^H, \{\beta_i\}_i^R, R \leq H$ in images I_0, I_1 which can not be well matched by SAM, assuming R area matches exist between the images:

$$As_l := \{A_{i\pi_l(i)}\}_i^R = \{(\alpha_i, \beta_{\pi_l(i)})\}_i^R \quad (9)$$

where As_l is a set of area matches, $\pi_l(i) \in [0, R)$ is an one-to-one permutation and l is the index of area matching possibilities. There are totally $L = \frac{H!}{(H-R)!}$ matching possibilities ($l \in [0, L)$), and only one true area match set (As_{l^*}) exists with the best geometry consistency:

$$P(As_l|l^*) = \delta(l - l^*) \quad (10)$$

where $P(As_l|l^*)$ is the correct probability of As_l , and δ subjects to $\delta(0) = 1$ and $\delta(x) = 0$, when $x \neq 0$. Based on Eq. 8, we can form the geometry consistency of As_l as:

$$G_{As_l} = \frac{1}{R} \sum_i^R G_{A_{i, \pi_l(i)}} \quad (11)$$

Algorithm 1: Geometric Area Match Rejector

Input: $As = \{A_{i\pi(i)}\}_i^S$
Output: $\{A_{i^*\pi(i^*)}, \mathcal{P}_{i^*}\}_i^T, i^* \in [0, S), T \leq S$

- 1 **for** $A_{i\pi(i)}$ **in** As **do**
- 2 get the correspondences: \mathcal{P}_i ;
- 3 calculate the fundamental matrix: F_i ;
- 4 get the self-geometry consistency by Eq. 6: $d_{i,i}$;
- 5 calculate the geometry consistency threshold:
 $T_{GR} = \phi \times \frac{1}{S} \sum_i^S d_{i,i}$;
- 6 **for** $A_{i\pi(i)}$ **in** As **do**
- 7 calculate the area match geometry consistency by
 Eq. 8: $G_{A_{i,\pi(i)}}$;
- 8 **if** $G_{A_{i,\pi(i)}} > T_{GR}$ **then** reject $A_{i\pi(i)}$;
- 9 **Output** the left area matches and their
 correspondences:
 $\{A_{i^*\pi(i^*)}, \mathcal{P}_{i^*}\}_i^T, i^* \in [0, S), T \leq S$;

which can be further written in probabilistic form:

$$P(G|As_l) = \exp(-G_{As_l}) \quad (12)$$

Therefore, the true match set can be achieved by geometry consistency maximization:

$$As_{l^*} = \operatorname{argmax}_{As_l} P(G|As_l) \quad (13)$$

Based on Eq. 10, this can be solved by considering the whole density of As_l and maximizing the weighted geometry consistency summation:

$$As_{l^*} = \operatorname{argmax}_{l^*} \sum_l^L P(G|As_l)P(As_l|l^*) \quad (14)$$

By solving Eq. 14, we can determine the true area match set As_{l^*} from the ambiguity. The analysis of GP computation complexity can be found in the supplementary material.

B. Geometry Area Match Rejector

After prediction, GAM Rejector (GR) further utilizes geometry consistency to reject potential false matches and improve the matching accuracy. Given an area match set $As = \{A_{i\pi(i)}\}_i^S$ achieved by SAM and GP, the geometry consistency of each $A_{i,\pi(i)}$ can be measured by $G_{A_{i,\pi(i)}}$ (Eq. 8). Then we can reject false or inaccurate matches with $G_{A_{i,\pi(i)}}$ greater than a certain threshold. In practice, the threshold T_{GR} is based on the mean self-geometry consistency (Eq. 6) with a weight ϕ . The Transformer-based matcher [9], [14] is embedded in GR to acquire precise point matches. The specific process is illustrated in Algorithm 1.

VI. AREA TO POINT MATCHING IMPLEMENTATION

In sum, the overall flow of the A2PM framework is as follows. First, the putative area matches ($\{A_{i,\pi(i)}^*\}_i^K$) and doubtful areas ($\{\alpha_i\}_i^H, \{\beta_i\}_i^R, R \leq H$) between images are achieved by SAM from semantic segmentation images (I_0^s, I_1^s).

$$\{A_{i,\pi(i)}^*\}_i^K, \{\alpha_i\}_i^H, \{\beta_i\}_i^R = SAM(I_0^s, I_1^s) \quad (15)$$

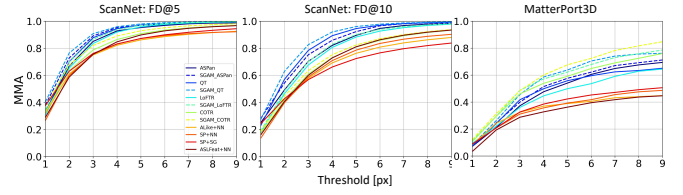


Fig. 3. **The image of MMA.** Our SGAM methods in this figure are implemented with their best parameter settings and significantly increases the matching accuracy for all direct matchers.

Then the doubtful areas are cropped from images (I_0, I_1) and matched by GP with PM, assuming R matches exist:

$$\{A_{i,\pi(i)}^*\}_i^R = GP_{PM}(\{\alpha_i\}_i^H, \{\beta_i\}_i^R, I_0, I_1) \quad (16)$$

Finally, the accurate area and point matches are achieved by GR with PM ($T \leq K + R$):

$$\{A_{i,\pi(i)}, \mathcal{P}_i\}_i^T = GR_{PM}(\{A_{i,\pi(i)}^*\}_i^{K+R}, I_0, I_1) \quad (17)$$

Under the same input image size, \mathcal{M}_A is more efficient than \mathcal{M}_D in most cases and detailed description can be found in the supplementary material.

VII. RESULTS

A. Dataset

To demonstrate the superiority of A2PM framework and SGAM method, we evaluate our methods (Implementation details can be found in supplementary material.) on two different datasets, ScanNet [43] and MatterPort3D [44], with their semantic labels as the input of SAM. The ScanNet contains numerous sequence images. We sample image pairs with various matching difficulties according to the frame difference from its *scene_0000* to *scene_0299* to evaluate our method. Due to the data collection settings of MatterPort3D, image pairs with overlap in this dataset have wide baseline leading to challenging matching which can be used to demonstrate our method performance under difficult matching conditions.

B. Point Matching

We construct point matching experiments on ScanNet and MatterPort3D for matching precision evaluation. For ScanNet, we construct two matching difficulties with image pairs under various *Frame Differences* (frame differences are 5 and 10, FD@5/10), each including 1500 image pairs. For the more challenging matching condition, 500 image pairs are sampled from the first 10 scenes in MatterPort3D.

Compared methods. We compare the proposed A2PM framework with conventional matching frameworks including detector-based matching and direct matching. For A2PM framework, we combine SGAM with present Transformer-based direct matching methods: SGAM_ASpan [16], SGAM_QT [15], SGAM_LoFTR [9] and SGAM_COTR [14] and compare different variations with various GAM parameters $\phi = 1 \sim 4.5$. In point matching framework, we choose the original ASpan [16], QT [15], LoFTR [9] and COTR [14] for direct matching. For detector-based matching, we select SuperPoint [24] with nearest

TABLE I

VALUE RESULTS (%) OF MMA. WE REPORT MMAS WITH DIFFERENT THRESHOLDS UNDER VARIOUS MATCHING DIFFICULTIES. THE OVERALL BEST RESULTS ARE **BOLD**. WE IMPLEMENT DIFFERENT VARIANTS OF SGAM ($\phi = 1 \sim 4.5$) FOR DIFFERENT POINT MATCHERS AND REPORT THE BEST RESULTS, WHICH ACQUIRE NOTEWORTHY PRECISION IMPROVEMENT.

MMA	ScanNet: FD@5		ScanNet: FD@10		MatterPort3D	
	MMA@1	MMA@2	MMA@2	MMA@3	MMA@4	MMA@5
SP [24]+NN	27.44	60.88	40.46	59.49	37.21	41.68
SP [24]+SG [33]	39.27	64.17	43.32	57.57	36.37	40.43
ASLFeat [11]+NN	28.89	58.85	40.98	60.41	34.39	38.78
ALike [10]+NN	32.84	61.77	40.76	58.34	37.51	38.95
Aspan [16]	32.99	66.91	49.83	70.79	47.66	54.06
SGAM_Aspan ($\phi = 2.5$)	37.88	72.81	54.67	75.42	51.49	57.61
QT [15]	32.79	70.40	56.92	78.46	49.89	55.82
SGAM_QT ($\phi = 2.5$)	39.43	75.96	62.49	82.32	58.59	63.75
LoFTR [9]	31.40	66.40	46.78	67.90	45.16	50.53
SGAM_LoFTR ($\phi = 1.5$)	35.26	70.61	48.50	70.25	56.44	61.59
COTR [14]	34.19	64.67	42.36	60.99	53.90	59.12
SGAM_COTR ($\phi = 1.5$)	38.70	68.97	46.47	65.43	60.06	67.61

neighbor matching (SP+NN) and with the learning matching SuperGlue [33] (SP+SG). The recent *SOTA* ASLFeat [11] and ALike [10] (ASLFeat+NN, ALike+NN) are compared as well.

Evaluation protocol. Following [23], [10], we report the mean matching accuracy (MMA@ i) in percentage under integer thresholds $i \in [0, 9]$ of each method and the number of matches is set as 500 for each method.

Results. Fig. 3 reports the MMA image which summaries the overall best MMA results achieved by A2PM framework with $\phi = 1.5$ for SGAM.LoFTR, SGAM.COTR and $\phi = 2.5$ for SGAM.Aspan and SGAM.QT. More representative MMA values are reported in Tab. I. It can be seen that A2PM framework boosts the matching precision of all direct matching methods significantly. Note ScanNet is the training dataset of Aspan, QT and LoFTR. Even so, SGAM still brings impressive accuracy improvement for them. On MatterPort3D dataset, SGAM achieves pronounced precision improvement especially in large MMA thresholds and outperforms other methods with a noteworthy margin, demonstrating the effectiveness of A2PM framework in challenging matching. Generally, SGAM with $\phi = 1.5$ obtains best results for COTR and LoFTR. As Aspan and QT are more accurate, SGAM with $\phi = 2.5$ can obtain better results. The specific ablation study of ϕ can be found in Sec. VII-F.0.b. In sum, owing to the proper search space, which alleviates many matching challenges, and more detailed input for point matcher in A2PM framework, SGAM significantly improves the matching accuracy for *SOTA* direct point matchers. More qualitative results can be found in the supplementary material.

C. Relative Pose Estimation

Accurate matches do not necessarily lead to accurate geometry, where point distribution is also important. Thus we next evaluate our method on the same datasets for relative pose estimation. We also sample 2×1500 image pairs from ScanNet (FD@5/10) and 500 image pairs from

MatterPort3D to construct three difficulties.

Evaluation protocol. Following [9], [33], we report the pose estimation AUC. The camera pose is recovered by solving the essential matrix with RANSAC. For ScanNet, we report the pose AUC@5°/10°/20°. As pose estimation is hard in MatterPort3D, we report the pose AUC@10°/20°/30°. The comparison and parameter settings are the same as in the point matching experiment.

Results. The pose AUC results are summarised in Tab. II. It can be seen that A2PM framework outperforms other frameworks with a notable margin on ScanNet, but most of the best pose estimation results are achieved with large $\phi = 2.5$ which can be interpreted as pose accuracy is determined by both the matching accuracy and the distribution of matches. Although SGAM assists PM to obtain precise point matches, it also makes point matches aggregate. Especially when the number of area matches is too few, tightly clustered points leads to inexact pose estimation. Thus, when the rejection threshold is relaxed to permit more area matches, A2PM framework can increase the pose estimation precision through more accurate point matches. For more challenging MatterPort3D dataset, our method is also able to bring impressive precision improvement which proves its better performance under difficulty scene.

D. Area Matching

We also evaluate SGAM on ScanNet dataset [43] for area matching performance. We sample 1500 image pairs under three matching difficulties (FD@5/10/30) respectively in ScanNet. The performance of SAM and SGAM combined with different point matchers are compared to show the importance of GAM.

Evaluation protocol. To measure the area matching accuracy, we propose two area matching metrics as follows.

1) *Area Overlap Ratio (AOR)*. This metric is to evaluate the single area match accuracy and achieved by projecting points ($\{p_i\}_i^N$) of $\alpha \in I_0$ to I_1 and getting the proportion of points falling into the matched area $\beta \in I_1$.

$$AOR(A) = \frac{1}{N} \sum_i^N (C(P(p_i), \beta)) \quad (18)$$

where the area match $A = (\alpha, \beta)$, $P(p_i)$ is projecting point p_i to I_1 , $C(q_i, \beta)$ is 1 when $q_i \in \beta$, otherwise 0.

2) *Area Matching Precision@t (AMP@t)*. Given all area matches $\{A_{i,\pi(i)}\}_i^M$ and a specific threshold $t \in [0, 1]$, this metric is the proportion of area matches whose $AOR > t$, evaluating the overall matching accuracy.

$$AMP@t = \frac{1}{M} \sum_i^M F(A_{i,\pi(i)}, t) \quad (19)$$

where $F(A_{i,\pi(i)}, t)$ is 1 when $AOR(A_{i,\pi(i)}) > t$, otherwise 0.

Results. The area matching results are summarised in Tab. III. The threshold t of AMP is changed with matching difficulty and set as 0.8, 0.7 and 0.6 severally. We report

TABLE II

RELATIVE POSE ESTIMATION RESULTS (%). THE POSE ESTIMATION AUC ON SCANNet (FD@5/10) AND MATTERPORT3D WITH THRESHOLDS 5° , 10° , 20° , 30° ARE REPORTED. THE OVERALL BEST RESULTS ARE **BOLD**. THE IMPRESSIVE RESULTS MANIFESTS THE EFFECTIVENESS OF A2PM FRAMEWORK AND SGAM METHOD IN POSE ESTIMATION.

PoseAUC	ScanNet: FD@5			ScanNet: FD@10			MatterPort3D		
	AUC@ 5°	AUC@ 10°	AUC@ 20°	AUC@ 5°	AUC@ 10°	AUC@ 20°	AUC@ 10°	AUC@ 20°	AUC@ 30°
SP [24]+NN	63.07	70.83	85.41	53.19	64.46	73.99	13.82	24.09	35.26
SP [24] +SG[33]	67.46	76.46	86.61	53.11	64.47	73.58	16.39	29.54	37.61
ASLFeat [11]+NN	68.08	75.64	85.66	56.89	68.66	78.33	12.64	25.91	39.26
ALike [10]+NN	69.67	78.29	83.46	50.29	61.27	70.31	15.14	20.03	23.79
ASpan [16]	72.88	80.40	84.70	58.51	70.42	79.84	18.35	27.81	43.98
SGAM_ASpan ($\phi = 2.5$)	73.60	81.52	85.83	60.78	74.24	84.53	20.50	30.08	48.49
QT [15]	71.35	76.14	77.90	59.27	69.77	74.96	16.53	26.98	39.96
SGAM_QT ($\phi = 2.5$)	72.55	77.69	79.57	61.82	71.83	76.82	18.90	28.11	42.21
LoFTR [9]	67.69	74.29	78.45	58.71	69.81	78.99	17.98	27.79	38.19
SGAM_LoFTR ($\phi = 2.5$)	71.22	79.31	84.44	59.50	73.12	83.13	18.14	32.28	45.37
COTR [14]	66.91	74.11	78.48	51.92	63.36	72.55	17.80	25.08	34.08
SGAM_COTR ($\phi = 2.5$)	70.18	78.22	83.22	53.99	66.29	77.17	19.20	28.31	41.25

TABLE III

AREA MATCHING PERFORMANCE ON SCANNet. THE AREA MATCHING RESULTS (%) OF SAM AND SGAM COMBINED WITH DIFFERENT POINT MATCHERS UNDER THREE MATCHING DIFFICULTIES IN SCANNet ARE REPORTED. THE OVERALL BEST RESULTS ARE **BOLD**. THE AREA MATCHING RESULTS MANIFEST THE EFFECTIVENESS OF SAM AND GAM. THE ACCURACY OF PM ALSO AFFECTS THE PERFORMANCE OF SGAM.

Area Match	FD@5		FD@10		FD@30	
	AOR	AMP@0.8	AOR	AMP@0.7	AOR	AMP@0.6
SAM	84.95	86.09	84.52	88.71	69.46	77.57
SGAM_ASpan ($\phi = 2.5$)	89.54	91.76	84.38	92.87	72.29	83.86
SGAM_QT ($\phi = 2.5$)	91.40	96.57	87.69	97.57	79.95	93.69
SGAM_LoFTR ($\phi = 1.5$)	90.03	92.31	85.46	93.07	72.56	85.04
SGAM_COTR ($\phi = 1.5$)	89.41	90.23	84.62	89.25	70.03	79.42

the results of SGAM combined with present SOTA direct point matchers with their best ϕ settings. In the table, the area matching precision of SAM decreases as matching get more difficult, but AMP values show most of the areas are matched accurately in all conditions. SGAM increases all the area matching accuracy proving the importance of GAM in area matching. The best area matching results are achieved by SGAM_QT, which is consistent with the point matching experiment. The parameter ϕ also affects the accuracy and should be set large to avoid rejecting precise matches when point matcher is accurate.

E. Understanding SAM

In SAM, areas are divided into semantic object area and semantic intersection area (SOA and SIA). We construct experiments to respectively evaluate the contributions of these two areas to area matching on ScanNet by their quantities and matching accuracy. The results are summarised in the first two rows of Tab. IV. As we can see, matching SOA is more accurate than matching SIA, due to the better stability of the centered object semantic against various matching noises. But the overall precision and quantity values reveal the importance of both areas in area matching.

TABLE IV

AREA MATCHING PERFORMANCE ON SCANNet OF TWO SAM AREAS AND GP. WE CONSTRUCT AREA MATCHING EXPERIMENTS FOR TWO AREAS IN SAM AND GP INTEGRATED WITH TWO POINT MATCHERS. AOR AND AMP@0.7 UNDER DIFFERENT MATCHING DIFFICULTIES (EACH WITH 1500 IMAGE PAIRS) ARE REPORTED ALONG WITH THE AREA NUMBER PER IMAGE.

	FD@5			FD@10			FD@30		
	AOR	AMP@0.7	num/img	AOR	AMP@0.7	num/img	AOR	AMP@0.7	num/img
SOA	85.94	94.10	3.13	85.26	91.76	2.91	70.84	68.36	2.30
SIA	83.67	91.91	2.38	83.50	84.35	2.01	66.94	62.17	1.26
GP_ASpan	86.59	96.70	0.255	84.83	89.59	0.355	81.26	86.97	0.502
GP_QT	87.86	96.82	0.255	84.98	88.47	0.355	82.37	87.91	0.502
GP_LoFTR	86.46	95.27	0.255	86.58	89.37	0.355	73.12	82.59	0.502
GP_COTR	87.51	95.73	0.255	87.42	92.18	0.355	73.81	86.48	0.502

F. Understanding GAM

a) *GP Precision.*: We investigate area matching performance of GP on ScanNet [43] under three difficulties (each with 1500 image pairs). The results are shown in the last two rows of Tab. IV. As we can see that the area matching precision of GP with both point matchers are higher than SAM especially when matching is difficult, demonstrating the effectiveness and importance of GP. Different point matchers also affect GP performance, as better point matching performance results in higher area matching accuracy. The area number per image (which does not change with point matchers) shows that the semantic ambiguity is non-trivial in SAM, which occurs more frequently as the matching difficulty increase. In sum, GP is an important part of SGAM which handles the semantic ambiguity and improves the area matching performance.

b) *Ablation study of GR parameter.*: To investigate the effect of the parameter ϕ in GR on point matching and pose estimation performance more carefully, experiments are constructed on ScanNet with three difficulties (FD@5/10/30) and each includes 1500 image pairs. The results are reported in Fig. 4. We can see that small ϕ favors point matching as strict rejection eliminates areas containing inaccurate point matches, but the resulting point aggregation degrades pose estimation accuracy. Also, although the best pose estimation

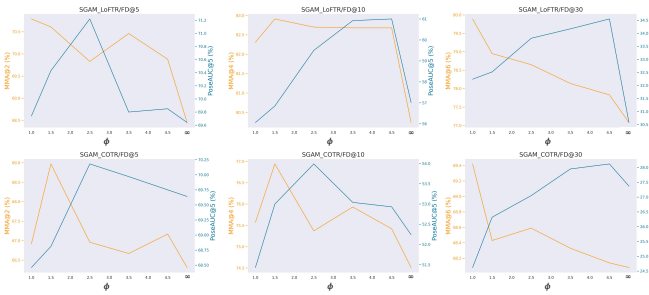


Fig. 4. **Ablation study of GR parameter ϕ .** The point matching and pose estimation performance of SGAM.COTR/LoFTR with different ϕ settings under three difficulties on ScanNet are reported. The blue lines are pose estimation accuracy and yellow lines correspond to point matching accuracy. The different values of ϕ are on the x-axis where ∞ represents SGAM w/o GR, permitting all area matches (zoom in for details).

is achieved by large ϕ , poor pose estimation results occur in the absence of GR. So the pose estimation performance is determined by both the accuracy and the distribution of point matches. Thus ϕ should be set with a balance of point matching precision and aggregation.

G. Limitations

Although SGAM is able to establish accurate area matches between images, heavily relying on semantic leads to limitations yet. For example, when the single semantic dominates the image, it is hard for SAM to find areas with clustered feature. That is to say, the main limitation of SGAM is related to the spatial granularity of semantic category. Hence the effectiveness of SGAM is restricted when semantic information, such as some large scale architectural scenes in SfM tasks. However, in such scenes, the A2PM framework is still benefit for feature matching, but the area matches needs to be established by other approaches similar to overlap estimation [41].

VIII. CONCLUSION

In this paper, a hierarchical feature matching framework, A2PM, is introduced, which aims at a reasonable search space for feature matching. By appropriately reducing the matching search space to semantic area matches, this framework allows for more precise point matching and alleviates the accuracy limitation of SOTA matching methods. To realize this framework, we further propose SGAM, an area matching method, which includes SAM and GAM. The SAM performs area matching roughly based on semantic cues. Then, the GAM, integrated with a point matcher, refines the area matches by geometry consistency and obtains accurate point matches. Extensive experiments manifest the effectiveness of our approaches, significantly outperforming other methods in image matching and pose estimation.

REFERENCES

[1] C. Cadena, L. Carlone, H. Carrillo, Y. Latif, D. Scaramuzza, J. Neira, I. Reid, and J. J. Leonard, “Past, present, and future of simultaneous localization and mapping: Toward the robust-perception age,” *IEEE Transactions on Robotics*, vol. 32, no. 6, pp. 1309–1332, 2016.

[2] J. L. Schonberger and J.-M. Frahm, “Structure-from-motion revisited,” in *Proceedings of the IEEE conference on computer vision and pattern recognition*, 2016, pp. 4104–4113.

[3] P. Truong, S. Apostolopoulos, A. Mosinska, S. Stucky, C. Ciller, and S. D. Zanet, “Glampoints: Greedily learned accurate match points,” in *Proceedings of the IEEE/CVF International Conference on Computer Vision*, 2019, pp. 10 732–10 741.

[4] D. G. Lowe, “Distinctive image features from scale-invariant keypoints,” *International journal of computer vision*, vol. 60, no. 2, pp. 91–110, 2004.

[5] E. Rublee, V. Rabaud, K. Konolige, and G. Bradski, “Orb: An efficient alternative to sift or surf,” *2011 International conference on computer vision*, pp. 2564–2571, 2011.

[6] A. Vaswani, N. Shazeer, N. Parmar, J. Uszkoreit, L. Jones, A. N. Gomez, Ł. Kaiser, and I. Polosukhin, “Attention is all you need,” *Advances in neural information processing systems*, vol. 30, 2017.

[7] J. Ma, X. Jiang, A. Fan, J. Jiang, and J. Yan, “Image matching from handcrafted to deep features: A survey,” *International Journal of Computer Vision*, vol. 129, no. 1, pp. 23–79, 2021.

[8] I. Rocco, M. Cimpoi, R. Arandjelović, A. Torii, T. Pajdla, and J. Sivic, “Neighbourhood consensus networks,” *Advances in neural information processing systems*, vol. 31, 2018.

[9] J. Sun, Z. Shen, Y. Wang, H. Bao, and X. Zhou, “LoFTR: Detector-free local feature matching with transformers,” *CVPR*, 2021.

[10] X. Zhao, X. Wu, J. Miao, W. Chen, P. C. Chen, and Z. Li, “Alike: Accurate and lightweight keypoint detection and descriptor extraction,” *IEEE Transactions on Multimedia*, 2022.

[11] Z. Luo, L. Zhou, X. Bai, H. Chen, J. Zhang, Y. Yao, S. Li, T. Fang, and L. Quan, “Aslfeat: Learning local features of accurate shape and localization,” *Computer Vision and Pattern Recognition (CVPR)*, 2020.

[12] I. Rocco, R. Arandjelović, and J. Sivic, “Efficient neighbourhood consensus networks via submanifold sparse convolutions,” *European conference on computer vision*, pp. 605–621, 2020.

[13] Q. Zhou, T. Sattler, and L. Leal-Taixe, “Patch2pix: Epipolar-guided pixel-level correspondences,” *CVPR*, 2021.

[14] W. Jiang, E. Trulls, J. Hosang, A. Tagliasacchi, and K. M. Yi, “Cotr: Correspondence transformer for matching across images,” in *Proceedings of the IEEE/CVF International Conference on Computer Vision*, 2021, pp. 6207–6217.

[15] S. Tang, J. Zhang, S. Zhu, and P. Tan, “Quadtree attention for vision transformers,” *ICLR*, 2022.

[16] H. Chen, Z. Luo, L. Zhou, Y. Tian, M. Zhen, T. Fang, D. McKinnon, Y. Tsin, and L. Quan, “Aspanformer: Detector-free image matching with adaptive span transformer,” in *Computer Vision—ECCV 2022: 17th European Conference, Tel Aviv, Israel, October 23–27, 2022, Proceedings, Part XXXII*. Springer, 2022, pp. 20–36.

[17] J. Yu, J. Chang, J. He, T. Zhang, J. Yu, and W. Feng, “ASTR: Adaptive spot-guided transformer for consistent local feature matching,” *CVPR*, 2023.

[18] D. Huang, Y. L. Ying Chen, S. X. Jianlin Liu, F. T. Wenlong Wu, Yikang Ding, and C. Wang, “Adaptive assignment for geometry aware local feature matching,” *CVPR*, 2023.

[19] J. L. Schönberger, M. Pollefeys, A. Geiger, and T. Sattler, “Semantic visual localization,” in *Proceedings of the IEEE conference on computer vision and pattern recognition*, 2018, pp. 6896–6906.

[20] Y. Bao, Z. Yang, Y. Pan, and R. Huan, “Semantic-direct visual odometry,” *IEEE Robotics and Automation Letters*, vol. 7, no. 3, pp. 6718–6725, 2022.

[21] B. Fan, J. Zhou, W. Feng, H. Pu, Y. Yang, Q. Kong, F. Wu, and H. Liu, “Learning semantic-aware local features for long term visual localization,” *IEEE Transactions on Image Processing*, vol. 31, pp. 4842–4855, 2022.

[22] K. M. Yi, E. Trulls, V. Lepetit, and P. Fua, “Lift: Learned invariant feature transform,” *European conference on computer vision*, pp. 467–483, 2016.

[23] M. Dusmanu, I. Rocco, T. Pajdla, M. Pollefeys, J. Sivic, A. Torii, and T. Sattler, “D2-net: A trainable cnn for joint description and detection of local features,” *Proceedings of the IEEE/CVF conference on computer vision and pattern recognition*, pp. 8092–8101, 2019.

[24] D. DeTone, T. Malisiewicz, and A. Rabinovich, “Superpoint: Self-supervised interest point detection and description,” *Proceedings of the IEEE conference on computer vision and pattern recognition workshops*, pp. 224–236, 2018.

[25] J. Revaud, C. De Souza, M. Humenberger, and P. Weinzaepfel, “R2d2: Reliable and repeatable detector and descriptor,” *Advances in neural information processing systems*, vol. 32, 2019.

- [26] M. Tyszkiewicz, P. Fua, and E. Trulls, "Disk: Learning local features with policy gradient," *Advances in Neural Information Processing Systems*, vol. 33, pp. 14 254–14 265, 2020.
- [27] A. Barroso-Laguna, E. Riba, D. Ponsa, and K. Mikolajczyk, "Key-net: Keypoint detection by handcrafted and learned cnn filters," *Proceedings of the IEEE/CVF International Conference on Computer Vision*, pp. 5836–5844, 2019.
- [28] G. Bökman and F. Kahl, "A case for using rotation invariant features in state of the art feature matchers," *Proceedings of the IEEE/CVF Conference on Computer Vision and Pattern Recognition*, pp. 5110–5119, 2022.
- [29] J. Lee, B. Kim, and M. Cho, "Self-supervised equivariant learning for oriented keypoint detection," *Proceedings of the IEEE/CVF Conference on Computer Vision and Pattern Recognition (CVPR)*, June 2022.
- [30] T. Ng, H. J. Kim, V. T. Lee, D. DeTone, T.-Y. Yang, T. Shen, E. Ilg, V. Balntas, K. Mikolajczyk, and C. Sweeney, "Ninjadesc: Content-concealing visual descriptors via adversarial learning," *Proceedings of the IEEE/CVF Conference on Computer Vision and Pattern Recognition*, pp. 12 797–12 807, 2022.
- [31] J. Revaud, V. Leroy, P. Weinzaepfel, and B. Chidlovskii, "Pump: Pyramidal and uniqueness matching priors for unsupervised learning of local descriptors," *Proceedings of the IEEE/CVF Conference on Computer Vision and Pattern Recognition*, pp. 3926–3936, 2022.
- [32] K. Li, L. Wang, L. Liu, Q. Ran, K. Xu, and Y. Guo, "Decoupling makes weakly supervised local feature better," *Proceedings of the IEEE/CVF Conference on Computer Vision and Pattern Recognition*, pp. 15 838–15 848, 2022.
- [33] P.-E. Sarlin, D. DeTone, T. Malisiewicz, and A. Rabinovich, "Superglue: Learning feature matching with graph neural networks," *Proceedings of the IEEE/CVF Conference on Computer Vision and Pattern Recognition (CVPR)*, June 2020.
- [34] Z. Zhong, G. Xiao, L. Zheng, Y. Lu, and J. Ma, "T-net: Effective permutation-equivariant network for two-view correspondence learning," in *Proceedings of the IEEE/CVF International Conference on Computer Vision (ICCV)*, October 2021, pp. 1950–1959.
- [35] J. Zhang, D. Sun, Z. Luo, A. Yao, L. Zhou, T. Shen, Y. Chen, L. Quan, and H. Liao, "Learning two-view correspondences and geometry using order-aware network," in *Proceedings of the IEEE/CVF International Conference on Computer Vision (ICCV)*, October 2019.
- [36] L. Xinghui, H. Kai, L. Shuda, and V. P. Adrian, "Dual-resolution correspondence networks," *NIPS 2020*, pp. 17 346–17 357, 2020.
- [37] D. Tan, J.-J. Liu, X. Chen, C. Chen, R. Zhang, Y. Shen, S. Ding, and R. Ji, "Eco-tr: Efficient correspondences finding via coarse-to-fine refinement," *European Conference on Computer Vision*, pp. 317–334, 2022.
- [38] J. Bian, W.-Y. Lin, Y. Matsushita, S.-K. Yeung, T.-D. Nguyen, and M.-M. Cheng, "Gms: Grid-based motion statistics for fast, ultra-robust feature correspondence," *Proceedings of the IEEE conference on computer vision and pattern recognition*, pp. 4181–4190, 2017.
- [39] Y. Fu, P. Zhang, B. Liu, Z. Rong, and Y. Wu, "Learning to reduce scale differences for large-scale invariant image matching," *IEEE Transactions on Circuits and Systems for Video Technology*, 2022.
- [40] A. Barroso-Laguna, Y. Tian, and K. Mikolajczyk, "Scalenet: A shallow architecture for scale estimation," in *Proceedings of the IEEE/CVF Conference on Computer Vision and Pattern Recognition*, 2022, pp. 12 808–12 818.
- [41] Y. Chen, D. Huang, S. Xu, J. Liu, and Y. Liu, "Guide local feature matching by overlap estimation," in *Proceedings of the AAAI Conference on Artificial Intelligence*, vol. 36, no. 1, 2022, pp. 365–373.
- [42] R. Hartley and A. Zisserman, "Multiple view geometry in computer vision," *Cambridge university press*, 2003.
- [43] A. Dai, A. X. Chang, M. Savva, M. Halber, T. Funkhouser, and M. Nießner, "Scannet: Richly-annotated 3d reconstructions of indoor scenes," *Proc. Computer Vision and Pattern Recognition (CVPR)*, *IEEE*, 2017.
- [44] A. Chang, A. Dai, T. Funkhouser, M. Halber, M. Niessner, M. Savva, S. Song, A. Zeng, and Y. Zhang, "Matterport3d: Learning from rgb-d data in indoor environments," *International Conference on 3D Vision (3DV)*, 2017.